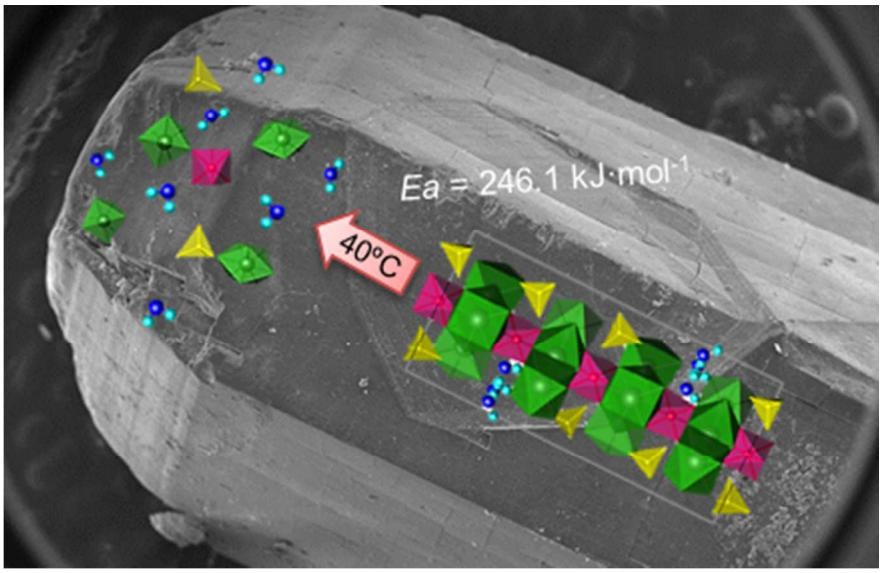

Reletionship between crystallinity and stability of ettringite
73x47mm (150 x 150 DPI)

Thermal stability of ettringite exposed to atmosphere: implications for the uptake of harmful ions by cement

Amalia Jiménez and Manuel Prieto*

Departamento Geología, Universidad de Oviedo, 33005 Oviedo, Spain

*corresponding author: amjimenez@uniovi.es

Address: Jesus Arias de Velasco s/n, 33005 Oviedo (Spain)

Phone: +34 985109552

Fax: +34985103103

KEYWORDS: ettringite, thermal behavior, decomposition kinetics, calorimetry, thermo-XRD.

ABSTRACT: The decomposition behavior of ettringite, $Ca_6Al_2(SO_4)_3(OH)_{12}\cdot 26H_2O$, at different temperatures was studied by means of isothermal XRD experiments, in which the evolution of the solid is monitored as a function of time. The experiments were performed at 40, 50, 55, and 60 ºC for a natural ettringite specimen. The experimental data were used to construct a Temperature-Transformation-Time (TTT) diagram. Such a diagram enables the prediction of the reaction pathways during the transformation process. The decomposition behavior was also studied under non-isothermal conditions using thermogravimetry and differential scanning calorimetry, and the obtained results were correlated with the results of the XRD study. Finally, the transformation kinetics and the activation energy (Ea = 246.1 kJ·mol^{-1}) of the reaction were estimated using the so-called "time to a given fraction" method. The temperature at which the initial transformation stage occurs (lower than 50ºC) indicates that ettringite cannot be considered a suitable host phase for the immobilization of radionuclides and other harmful elements, as is frequently proposed in the literature.

INTRODUCTION

Ettringite occurs in natural alkaline environments that are associated with silicates, calcite and phosphates. [1-2] Ettringite is a rare mineral, being neither ubiquitous nor abundant. However, a non-natural analog of ettringite forms via hydration of calcium aluminates[3] when gypsum is added during the early hydration of Portland cements, which explains the environmental relevance given to this mineral. Portland and modified Portland cements are useful matrices for the immobilization and storage of contaminants contained

in various forms of hazardous wastes[4-6] ettringite is frequently assumed to play a key role in these immobilization processes. After the pioneering work of Bannister et al.[7], the crystal structure of ettringite has been the subject of numerous detailed studies[3,8-10] Hartman and Berliner[8], using time-of-flight neutron powder diffraction techniques, refined the structure of ettringite in the P31*c* space group with $a \approx 1.116$ nm and $c \approx 2.135$ nm (at 10K). The calculated heavy atom positions are essentially the same as those obtained in previous investigations, but in addition this study provides the precise hydrogen atom positions, revealing the arrangement of the hydrogen bonding network in the structure. Moreover, a comparative study on the crystal structure of wet and dried ettringite reveals that the amount of structural water, the point symmetry of sulfate and the hydrogen bond network are analogous in both cases[11]. Although ettringite is typically described by the general formula $Ca_6Al_2(SO_4)_3(OH)_{12}\cdot 26H_2O$, the exact water content varies because it can include adsorbed water in addition to structural water.[3] The basic structural framework consists of alternating calcium and aluminum coordination polyhedra, i.e., $Ca(OH)_4(H_2O)_4$ and $Al(OH)_6$, that form 'columns' parallel to the c-axis. Water molecules and sulfate tetrahedra occupy the wide channels located between these columns and are connected by an extensive network of hydrogen bonds, which are responsible for the structural stability. Due to these features, the ettringite structure is flexible enough to accommodate foreign cations and oxyanions.

Ettringite is usually considered a remarkable host phase for the sequestration of radionuclides[12] and other harmful ions. The crystal structure of ettringite favors the substitution of SO_4^{2-} by other oxyanions, such as chromate, arsenate, selenate, selenite, vanadate, molibdate, and stannate.[13-18]Moreover, the substitution of Ca^{2+} by divalent

cations (Pb^{2+}, Cd^{2+}, Co^{2+}, Ni^{2+}, etc.) at the M^{2+} site is largely known.[19] Such availability for ionic substitution suggests that ettringite-based solid-solution formation can be one of the most effective mechanisms for immobilization of toxic cations and oxyanions in cements. Cement maintains a high buffering reserve of alkalinity[4], which reduces the solubility of the ettringite host phase and hence the 'solubility' of the foreign substituting ions.

The best scenario for immobilization of pollutant ions by co-crystallization is to have a low solubility related to a robust controlling phase.[12,20,21] The question is whether ettringite can be considered a 'robust' phase or not. In fact, the thermal stability of ettringite appears to be quite limited. The mechanism of decomposition of ettringite has been the subject of a number of studies[22-26], but some important aspects are still under discussion. In the presence of liquid water, the stability limit of ettringite is clearly established to be ~120 ºC[22]. However, ettringite is thermally unstable at much lower temperatures in contact with the atmosphere, particularly at low water vapor pressures, when water is present mainly as 'crystal water'. During the decomposition process, there appears to be a simultaneous loss of hydroxyls and water molecules from the structure[8], which eventually leads to a product that is amorphous to X-rays, although the existence of metaettringite (a partially dehydroxylated product that still yields an electron diffraction pattern) has been reported.[23]

Although the structural changes occurring during the decomposition of ettringite are reasonably well established, it is not clear whether ettringite may decompose over the temperature-time range relevant to the performance of ettringite-based products in warm service environments.[22] Concrete service temperatures can exceed 40ºC in near-surface scenarios where severe insolation occurs, or in deep hot mines and nuclear waste repositories, where temperatures can attain values higher than 50ºC as a consequence of

both the geothermal gradient and the heat generated by high-level nuclear wastes.[27-30] For instance, Blanco-Martín[31] modelled the evolution of the temperature in a deep disposal in salt rocks and they assessed temperatures above 60ºC after few days of the radionuclides emplacement and peaks of temperature above 180ºC after about 1 year in different locations of the disposal. Clearly, all the previous results indicate that the thermal stability of ettringite is limited, but its decomposition kinetics at different temperatures is actually not very well known.

Pourched and co-workers[24] proposed a kinetic model for ettringite decomposition from isothermal and non-isothermal thermogravimetric measurements obtained at 50 ºC and 0.5 ºC/min, respectively. However, to our knowledge, a systematic thermo X-ray diffraction (XRD) study has not been performed yet. In most works, XRD patterns of the decomposition products are obtained *ex-situ* or are performed intermittently as the temperature is increased at a given heating rate. Unfortunately, while those previous studies are suitable to establish the decomposition sequence, they are unable to answer some practical questions such as "How long will ettringite remain stable at 40ºC in contact with the atmosphere?".

This work addresses the decomposition behavior of ettringite at specific temperatures through isothermal XRD experiments, in which the evolution of the diffractograms is monitored *in situ* as a function of time. The experiments were performed at 40, 50, 55, and 60ºC for a natural ettringite specimen. We previously demonstrated that this natural specimen was more resistant to dehydration than the typical synthetic samples, due to its better crystallinity. The aim was to select the most favorable starting material from the point of view of keeping stability. The experimental data were used to construct a

Temperature-Transformation-Time (TTT) diagram. Such a diagram allows for prediction of the reaction pathways during sub-solidus phase transformations and is commonly used in material and mineral sciences.[32] However, to our knowledge, TTT diagrams have not been applied to the decomposition processes involving solid and gas phases. The decomposition behavior was also studied under non-isothermal conditions by thermogravimetry and differential scanning calorimetry, and the obtained results were correlated with the results of the XRD study. Finally, the transformation kinetics and the activation energy of the process were estimated using the so-called "time to a given fraction" method.[32]

MATERIALS AND METHODS

Synthetic and natural samples

Synthetic ettringite was obtained following a modification of the method described by Perkins and Palmer[33] This procedure begins with the preparation of two reactant solutions by adding 6.65g of $Al_2(SO_4)_3 \cdot 18H_2O$ and 4.44 g of $Ca(OH)_2$ to 100 ml and 250 ml of deionized water, respectively. The two starting solutions were introduced in a glove-box with a nitrogen atmosphere, in which nitrogen was bubbled through the reactant solutions to avoid CO_2 contamination. After 24 hours, the reactant solutions were mixed in polypropylene beakers and adjusted to pH 11.5 with the addition of 0.5 ml of NaOH (1N). Next, additional deionized water (150 ml) was added to obtain 500 ml of a final solution with suitable molar ratios of $Ca/SO_4 = 2$ and $Ca/Al = 3$. The mixture was stirred at 400 rpm over 48 hours at 25 ± 0.5 ºC and maintained statically over two weeks in nitrogen atmosphere at 25ºC. After the reaction period, the precipitate was separated from the aqueous solution via centrifugation (6000 rpm) and subsequently filtered through 0.45 μm

filters. The precipitates were dried at room temperature in a desiccator to avoid dehydration.

The natural ettrinigite specimen was obtained from the N'Chwaning mine in Kuruman (South Africa), and consisted of single, light greenish and prismatic crystals approximately 8 mm in length and 3 mm in width.

Characterization of the ettringite samples

Both the synthetic and the natural samples were characterized by XRD. The natural specimen was first gently crushed by hand using an agate mortar to a fine powder of approximately 20μm in particle size, whereas the synthetic samples were analyzed as obtained after being dried in a desiccator at room temperature. The diffraction patterns were collected in a Philips X'Pert-PRO automatic diffractometer using CuKα radiation and scanning over the 2θ range of 5º to 60º. Indexing of the main reflections was made using the crystallographic analysis tools of the computer program X'Pert HighScore Plus (©2008, PANalytical B.V.). To investigate the crystallinity of the samples, the widths of some selected reflections were analyzed by considering the full width at half-maximum (FWHM) values. The smaller the FWHM values are, the larger the crystallite size is and the better is the crystallinity.[34] As is widely known, the crystallite size represents the size of the coherently diffracting domain and not the size of the precipitate particles. Here, the crystallite size of both samples was roughly estimated using the X'Pert Plus ''Scherrer calculator" tool.

Representative individuals of the synthetic and natural samples were imaged using a JEOL-6610 scanning electron microscope (SEM). The SEM is equipped with an INCA

Energy 350-Xmax 50 microanalysis system (EDS) with a SDD-Xmax 50 detector (INCA) and an ultra-thin window, which permits the detection and semi-quantitative analysis of light elements. This microanalysis system was used to estimate the chemical composition (Ca, S, and Al) of both natural and synthetic samples.

Thermal study: Thermogravimetry, DSC and Thermo-XRD

Thermogravimetric (TG) and derivative thermogravimetrial (DTG) analyses were performed with the ettringite samples (~20 mg of initial mass) using a Metter Toledo TGA/SDTA 851 thermal analyzer. All measurements were performed between 298 and 1273 K at a heating rate of 10 $K \cdot min^{-1}$ in a dynamic atmosphere, using a nitrogen flow rate of 50 ml/min. The temperature and weight precision of the apparatus were ± 0.25 K and ± 1 μg, respectively. A Pfeiffer Vacuum ThermoStar™ GSD301T mass spectrometer was used to analyze the gas phases released during the TG study. The masses 18 (H_2O) and 44 (CO_2) were tested by using a detector C-SEM, operating at 1400 V, with a time constant of 0.5 s.

The samples were also analyzed via Differential Scanning Calorimetry (DSC) using a Metter Toledo DCS 822e apparatus to determine the temperatures and enthalpies of dehydration. Heat-flow measurements were performed in the temperature range of 298-900 K under a flow of N_2 gas at a heating rate of 10 $K \cdot min^{-1}$. The initial mass of each sample was ~6 mg. Before characterizing the samples, the equipment was operated using indium and zinc standards to calibrate the temperature and heat flow. The temperature precision of the equipment was ± 0.2 K, and the reproducibility was ± 0.1 K.

The evolution of both the natural and the synthetic sample with increasing temperature was studied via *in situ* thermo-XRD using CuKα radiation on a PANalytical X'Pert Pro

175 powder diffractometer equipped with a PIXcel solid-state detector and a high temperature
176 chamber (Anton Paar HTK 1200 N). Diffractograms were collected over a $5 < 2\theta < 40^{\circ}$
177 range with a step size of 0.013º. All measurements were performed in static air atmosphere
178 by collecting the diffraction patterns at fixed temperatures (typically at 25ºC increments)
179 between 25ºC and 250ºC. The heating rate between two consecutive scans was 5 $K \cdot min^{-1}$.
180
181 **Isothermal XRD experiments**
182 The decomposition behavior of the natural specimen was studied via *in-situ* XRD
183 isothermal experiments using the PANalytical X'Pert Pro powder diffractometer previously
184 described. The sample was placed in a holder, which was introduced in a closed oven
185 chamber (Anton Paar HTK 1200N) at ambient conditions (25 ± 2ºC, relative humidity 60-
186 70%) and then brought to prefixed temperatures (40ºC, 50ºC, 55ºC or 60ºC). The heating
187 rate was 10 $K \cdot min^{-1}$, and once the temperature was reached, the sample was maintained at
188 isothermal conditions. The powder patterns in each isothermal series were collected in a
189 static air atmosphere at regular intervals of 5 min (during the first two hours), 1 hour
190 (during the first day) and 6 hours (from the second day). All the diffraction patterns were
191 scanned in the range of $8^{\circ} < 2\theta < 30^{\circ}$ with a step size of 0.001º. Every run was
192 duplicated, and the results were found to be reproducible. The decomposition of ettringite
193 with increasing time was checked by evaluating the peak area (A) in counts per second
194 (cps) of the first reflection (100) by using X´Pert Viewer. The transformation extent was
195 established from the ratio A_t/A_0, where A_0 and A_t correspond to peak areas at the beginning
196 of the experiment ($t = 0$) and at a given time (t), respectively.
197

RESULTS AND DISCUSSION

Characterization of the synthetic sample and the natural ettringite

Figure 1 shows the powder XRD patterns obtained for both the natural and the synthetic sample before the thermal treatment. As expected, both diffractograms fit the reference pattern of ettringite (PDF 00-041-1451; spatial group P31*c*). The main reflections can be indexed as 100, 110, 104, and 114 (with *d*-spacings of ~9.72, 5.61, 4.69, and 3.87 Å, respectively). In the case of the synthetic sample, other minor reflections appear, with *d*-spacings of ~7.63 and 4.28 Å, which can be assigned to the main reflections of gypsum (020 and 021 respectively). Atkins[35] also reported the gypsum impurities in their synthetic samples of ettringite. As can be observed, a broad reflection also appears at 2θ ~29.22º, which can be assigned to a combination of the main reflection of calcite (104) and the third most important reflection of gypsum (041) that typically occur at 2θ ~ 29.45 and 29. 11º, respectively. The occurrence of carbonate phases can be explained by the effect of CO_2 atmospheric[23] during handing of the samples but also by trace amounts of calcite in the reactant (CaOH) used in the synthesis of ettringite.

In summary, ettringite was found to be the only phase present in the natural sample, whereas a mixture of ettringite with minor amounts of gypsum, calcite and monocarbonate was identified in the synthetic sample. The initial experimental setup was designed to reach a pH value of 11.5, for which ettringite is the most stable phase. However, during aging (48 hours), the pH decreases until values close to 10.7 are reached, at which point ettringite and gypsum can co-precipitate.[14] The presence of gypsum may hence be a result of the compositional evolution of the parent solution during the experiment. These results can be

predicted by inputting the concentration and pH of the parent solution into geochemical codes, such as PHREEQC[36] or GEMS.[37] Using PHREEQC with the WATEQ4F database and the solubility data of Perkins and Palmer[33], the saturation index (SI) with respect to ettringite takes a value of ~19.9, which is therefore the most likely phase to precipitate. The parent solution was also supersaturated with respect to gypsum (SI = 0.78 > 0) and other metastable solid phases (monosulfate, portlandite, gibbsite, hydrogarnet), but only gypsum, calcite and monocarbonate were identified in the diffractograms.

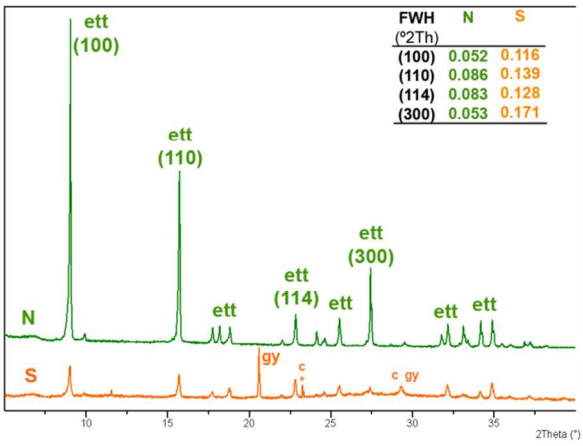

Figure 1. Powder XRD patterns of the natural (N) and synthetic (S) samples. Ettringite (ett) is the main phase in both samples, while gypsum (g), calcite (c) and monocarbonate (*) were identified as minor phases in the precipitate. FWHM values indicate (see inset) that the natural sample is more crystalline than the synthetic.

Secondary electron images show the elongated, prismatic habit of the ettringite crystals in both the natural and the synthetic sample (Figure 2). Although the habit is similar in both cases, the crystal sizes are clearly different. The crystals obtained by precipitation were found to be significantly smaller (~5μm long) than the natural ones (~8mm long). Semi-

quantitative EDS microanalyses of both the natural and the synthetic sample confirm that the mean Ca/S and Ca/Al atomic ratios are close to 3 and 2 respectively, which agree with the ettringite stoichiometry. The natural specimen appeared to be relatively pure since the presence of foreign elements was not detected via EDS-microanalyses.

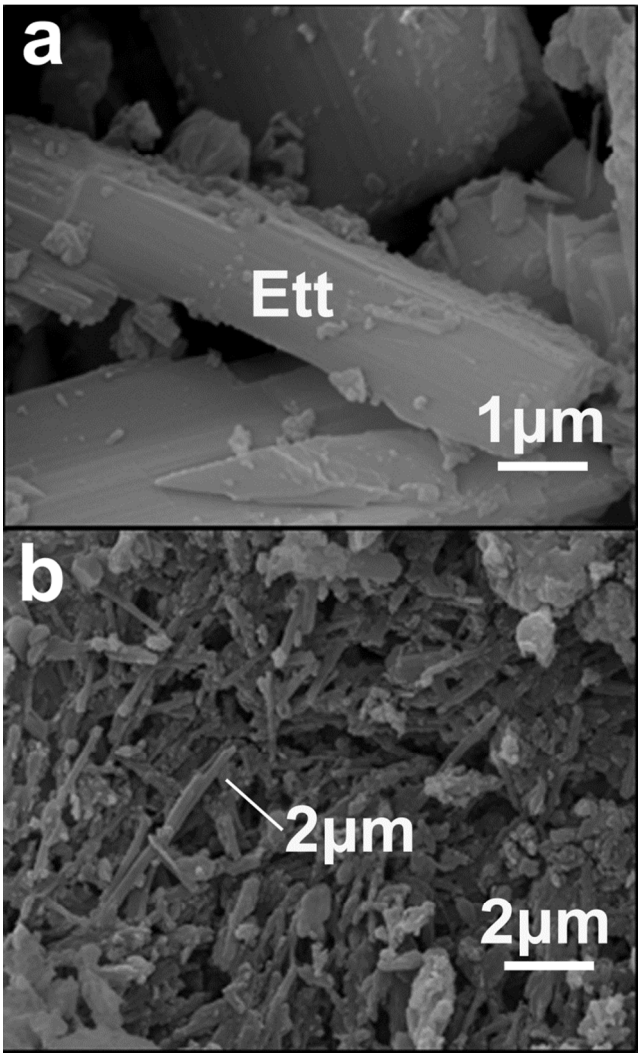

Figure 2. SEM images showing the elongated crystal habit of ettringite in the natural (a) and the synthetic (b) samples.

In the case of the natural sample, the refined unit cell parameters (a = 11.2530 Å and c = 21.6436 Å) are quite similar to those reported in the reference pattern (a = 11.2240 Å and c = 21.4080 Å). However, the cell parameters calculated for the synthetic sample (a = 11.2514 Å and c = 22.6788 Å), exhibit some differences. While the a-axis parameter is slightly smaller, the c-axis parameter is clearly larger. These results indicate that the columns of Ca-Al polyhedra along the c-axis[3] are slightly longer for the synthetic sample than for both the natural specimen and the reference pattern. Significant differences between the crystals in this study and the synthesized (a = 11.66881 Å and c = 21.5366 Å) by Hartman[8] were also observed. Both the crystal size and the crystal-chemistry appear to be influenced by the crystallization conditions of the precipitation experiments, which obviously differ from the typical conditions of ettringite formation in natural environments.

All the reflections were found to display smaller broadening and higher intensity in the natural sample than in the synthetic one (Figure 1). Inspection of the FWHM data indicates that the most intense 100 reflection is the most narrow (0.053 and 0.116 º 2Theta for the natural sample and the synthetic, respectively). In a polycrystalline sample, a variety of microstructural phenomena exist that lead to anomalous diffraction effects.[38] Peak broadening can be caused by a small crystallite size, the presence of crystal defects, lattice strain, or compositional heterogeneities.[39,40] Because ettringite is a stoichiometric phase, the broadening differences between both samples cannot be attributed to compositional heterogeneity. Based on the FWHM of the 100 reflections, the crystallite size can be estimated to be 126 nm and 69 nm for the natural and the synthetic sample, respectively. However, polycrystalline material usually contains other imperfections that can also produce broadening effects.[41] Unfortunately, determining the precise contribution of each

of the microstructural factors to the observed broadening is not straightforward.[42] In the case of ettringite, synthetic crystals are usually obtained at a high supersaturation and can be expected to incorporate a higher concentration of defects than natural crystals. Such is the case here, where the precipitation-aging experiments were performed under conditions that appear to affect the crystallinity (Figure 1), crystal habit and crystal size (Figure 2).

Dehydration behavior of ettringite

Although some thermal studies have been performed on natural ettringite[43], most research was performed using synthetic samples.[23, 25,26] A comparison between the thermal behavior of synthetic solids and natural specimens of higher crystallinity can provide further insight into this matter. With this aim, Figure 3 displays the thermogravimetric (TG) and derivative thermogravimetric (DTG) curves obtained for the natural (Figure 3a) specimen and the synthetic sample (Figure 3b). Mass spectrometry analyses of the amount of H_2O released from both samples at increasing temperatures are also shown. No significant quantities of CO_2 were detected in the released gases. Overall, the combination of these three curves (TG, DTG and H_2O) indicates that the weight loss observed in both the natural and the synthetic sample is due to the release of water molecules and/or hydroxyl groups.

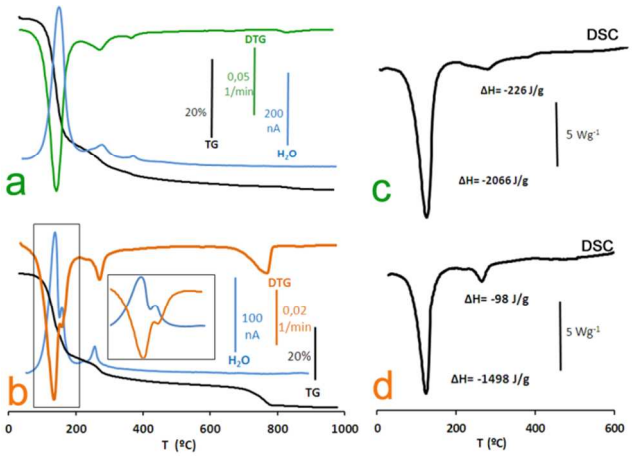

Figure 3. TG curves (black), DTG curves (green and orange) and H_2O (blue) depicting the release from natural (a) and synthetic (b) samples. DSC curves for natural (c) and synthetic (d) samples as a function of temperature.

Although the TG curves obtained for both samples exhibit a similar profile, a detailed study of the DTG curves indicates that differences exist between natural and synthetic sample. The natural sample undergoes a higher (45.5%) total weight loss than the synthetic one (40.50%) at the end of the TG analyses (1000ºC). Some features of the DTG curves, such as the temperature corresponding to the maximum weight-loss rate, also indicate differences in the dehydration behavior of both samples. The natural sample dehydrated in two separated stages (Figure 3a). The first stage occurs between 25-190ºC, with a total loss of ~33%, equivalent to 23 water molecules. The maximum weight-loss rate occurs at ~138ºC, corresponding to the release of ~16 water molecules from the sample. The second stage (190-300 ºC) involves a loss of ~4.5%, which corresponds to a release of ~3 water molecules at a maximum rate at ~274ºC. After the second stage, both the TG and DTG curves (Figure 3a) show a progressive weight loss (~7.5%) until the end of the experiment

(1000ºC).In the case of the synthetic sample, a double-step dehydration event occurs in the first stage, with a total loss of ~ 27% (~ 19 water molecules) between 25-190ºC. The DTG curve shows a maximum rate of weight loss at ~130 ºC and a shoulder at ~155 ºC. The shoulder could be explained by the presence of gypsum, which also dehydrates in two steps: The initial formation of bassanite ($CaSO_4 \cdot 0.5H_2O$) is closely followed by a second step, in which dehydration proceeds to completion, with anhydrite (α-$CaSO_4$) being the final anhydrous phase.[44] Here, the combined dehydration of gypsum and ettringite could explain the DTG behavior of the synthetic sample during the first stage. Dehydration of the ettringite component continues between 190-300 ºC, with a maximum rate at ~ 269 ºC and a total weight loss of ~ 5.6%. At the end of the second stage, the synthetic sample undergoes a total weight loss of ~32.6%. After complete dehydration, a new weight loss occurs between 650 and 800 ºC (Figure 3b), which can correspond to the decomposition of calcite identified by DRX (Figure 1).

The fact that the water molecules in ettringite occupy structural positions with different crystal-chemical roles[3] determines both the hydrogen bonding architecture and the homogenous distribution of the positive charges, which could favor a sequential release of the water molecules with increasing temperature. These crystallographic features would explain the different stages of weight loss observed in the TG/DTG experiments.[25,45,46] However, there is no evidence to exclude a more complex behavior involving the simultaneous loss of hydroxyl groups and water molecules.[26] The results of the DSC experiments do not clarify this matter. As seen in Figures 3c and 3d, the DSC curves show two main exothermic intervals below 300ºC. In the case of the synthetic sample, the DSC curve shows a double peak in the first interval. The enthalpy ΔH (J/g) and T (ºC) of the

328 exothermic peaks for each interval are displayed in the graphs. Note that the peak minima
329 in both intervals are less pronounced for the natural sample than for the synthetic one.
330 These results are in good agreement with the TG/DTG study and clearly support the idea
331 that the two exothermic peaks observed in the natural sample are related to the two stages
332 of dehydration/decomposition. In the case of the synthetic sample, the DSC curves confirm
333 the double-step behavior in the first temperature range (25-190ºC), which is attributed to
334 the presence of gypsum. Consequently, establishing the nature of the phases resulting from
335 the dehydration process requires complementary structural data.
336
337 **Thermal evolution of the XRD patterns**
338 Figure 4a displays a series of diffractograms obtained for the natural sample with
339 increasing temperature obtained via thermo-XRD experiments. The most important
340 reflections (100, 110, and 114) of ettringite are found to be fully preserved in the
341 diffractograms obtained up to 50ºC and can be clearly identified below 100ºC (Figure 4a).
342 Nevertheless, the reflections become less intense and undergo a progressive increase of
343 FWHM values, which indicates a decreasing degree of crystallinity with increasing
344 temperature (see Table 1). The thermal degradation of ettringite is generally considered to
345 represent the transition to an amorphous phase.[26] Although this new phase appears to be
346 amorphous according to the XRD results, it shows signs of crystallinity via electron
347 diffraction.[23] Such a new phase was termed meta-ettringite because it retains the columnar
348 structure of ettringite along the *c*-axis. The mechanism of collapse of ettringite to meta-
349 ettringite involves the loss of water molecules and possibly a rotation of individual cationic
350 columns, which results in the loss of crystallinity typical of meta-ettringite[22] at

351 temperatures approximately 115ºC. Figure 4a shows that ettringite reflections are no longer
352 recognized in the diffractograms obtained above 100ºC.

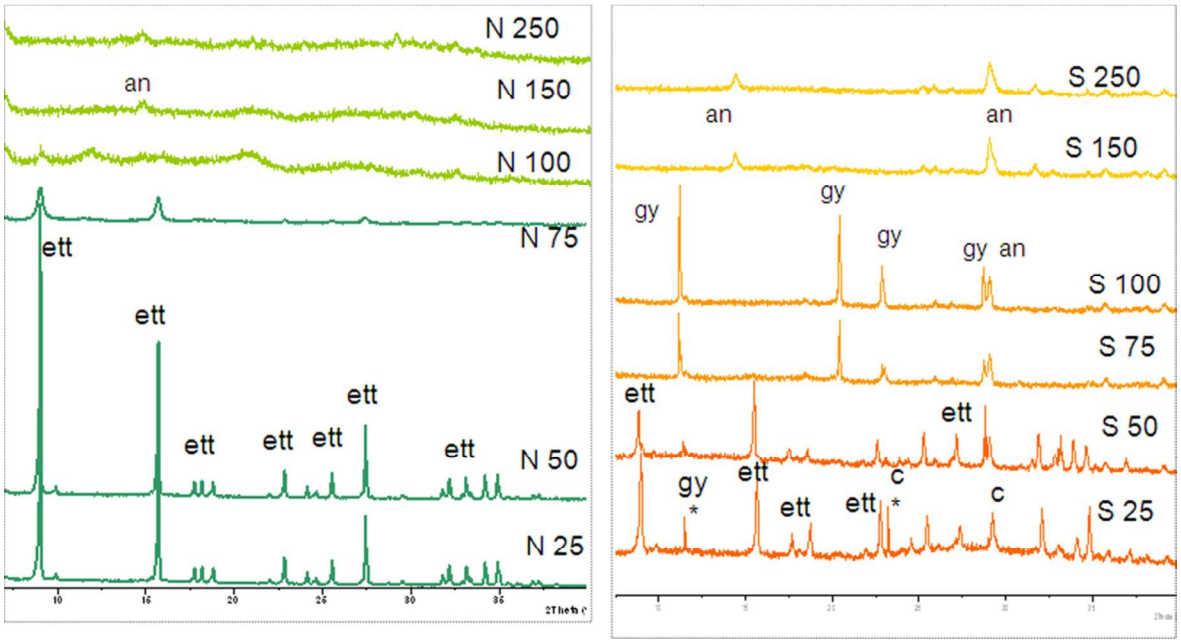

353

354 **Figure 4.** Selected powder XRD patterns obtained during thermal treatment of (a) natural
355 (N) and (b) synthetic samples (S). The numbers indicate the temperature in ºC. The
356 reflections are labelled as ettringite (ett), calcite (c), monocarbonate (*), gypsum (gy) and
357 anhydrite (an).

358

359 **Table 1.** Evolution of the crystallinity of ettringite during thermal treatment: broadening
360 (FWHM) and intensities (I) obtained for the main reflections identified in ettringite.

sample	T (ºC)	(001)		(110)	
		FWHM (°2Th)	I (counts)	FWHM (°2Th)	I (counts)
Natural	25	0.053	19423	0.086	9847
Natural	50	0.075	9258	0.087	9741
Natural	75	0.23	2635	0.306	788

Natural	100	0.33	42.3	0.305	42
Synthetic	25	0.152	852	0.139	1402
Synthetic	50	0.216	282	0.118	1305

Although the diffraction patterns obtained between 100ºC and 250ºC appear to correspond to a non-crystalline material, despite the poor crystallinity, some incipient reflections can be identified (Figure 4a). Thus, in the diffractograms obtained between 100ºC and 175ºC, the main reflections of gypsum (020 and 021) appear. In addition, some broad reflections observed between 75ºC and 250ºC can be identified (Figure 4a) as bassanite ($CaSO_4 \cdot 0.5H_2O$) and/or metastable γ-anhydrite ($CaSO_4$). Distinguishing bassanite from γ-anhydrite using conventional powder XRD is complicated due to the slight differences between their crystal structures.[47] The presence of gypsum, hemihydrate and/or anhydrite can be explained by the reaction between water molecules, sulfate and calcium ions to yield coherently diffracting domains of calcium sulfate phases within a matrix of amorphous material. Previous works[48,23] reported the formation of mixtures of gypsum, hemihydrate and monosulfate (AFm) at ~ 115 ºC. Here, monosulfate was not identified in any of the diffractograms obtained between 25ºC and 250ºC. Moreover, no crystalline aluminates were found, which indicates that the aluminum released from ettringite occurs as an amorphous phase containing aluminum.

Figure 4b shows a series of diffractograms obtained at increasing temperatures for the synthetic sample. Some important differences are found with respect to the series obtained with the natural sample. The main reflections of ettringite only appear in diffractograms obtained below 50 ºC, while they were present in the natural sample up to 100ºC. By comparing the values of width and intensity of the main reflections (Figure 1), it is clear

that the synthetic ettringite undergoes an earlier decrease of crystallinity during the heating process. Gypsum appears in the diffractograms obtained at temperatures below 125ºC, while bassanite/anhydrite reflections appear in the diffractograms obtained at higher temperatures.

In summary, the previous results indicate that the natural specimen is more resistant to dehydration than the synthetic sample. The natural sample was found to remain unaltered up to 75ºC; in contrast, for the synthetic sample, the ettringite reflections begin to vanish at a lower temperature (>50ºC). Such a different behavior can be explained by the smaller crystallinity degree of the synthetic sample, which is consistent with the small particle size of these precipitates. Low crystallinity is mostly due to a small crystallite size. The crystallite size is the size of a coherently diffracting domain and thus does not necessarily coincides with the particle size. However, tiny crystals precipitated at a high supersaturation normally exhibit small coherently diffracting domains and poor crystallinity. Therefore, the natural specimen appears to be the best choice to study the dehydration kinetics of ettringite and its implications in the role of this mineral as sequestering phase for harmful ions.

Dehydration kinetics

In-situ XRD isothermal experiments were performed different temperatures (40ºC, 50ºC, 55ºC and 60ºC) to determine the dehydration kinetics of ettringite. The study was focused on the first stage described in the previous section and was applied to the natural specimen, which was demonstrated to be a more 'robust' phase. Figure 5a shows the changes in the peak area (A) of the main XRD reflection of ettringite (100) as a function of time during

405 the isothermal experiments. The peak area decreases quickly during the early hours and
406 then slowly evolves towards an asymptotic value. The trend is the same in all the
407 experiments, which indicate that the same transformation mechanism is operating at the
408 studied temperatures. A quantitative estimation of the transformation extent was
409 determined from the ratio A_t/A_0. The time (t) to transform a fraction of ettringite (Y_{10}) of
410 approximately 10% was calculated (see inset in Figure 5b). The decrease in the peak area
411 observed in the isothermal experiments is consistent with the initial decomposition stage,
412 which involves dehydration (Figure 4) and a loss of crystallinity (Table 1). Nucleation,
413 growth and transformation of gypsum and anhydrite occur during the second stage of the
414 thermal treatment (Figure 4) and are not considered here.

415 The experimental values obtained at different temperatures for the time (t) at which the
416 fraction transformed was Y_{10} can be used to estimate the activation energy (Ea) via the
417 method of "time to given fraction".[32] This method establishes that the transformed fraction
418 (Y) and time (t) are related by a function in which the dependent variable is t instead of the
419 kinetic constant (k). Hence, the strong dependence of the "kinetic constant" procedure is
420 avoided. When the mechanism does not change over the temperature range studied, t_Y can
421 be described by the expression:

422 $$t_Y = A^{-1} \cdot e^{\left(Ea/RT\right)}, \quad (1)$$

423

424 Where A is a fitting constant, R the gas constant, and T the temperature in Kelvin. In
425 practice, the experimental data can be plotted as shown in Figure 5b, where $\ln t_{0.1}$ is
426 represented on the ordinate against $1/T$ on the abscissa. The slope of the straight line fitting
427 these data-points corresponds to Ea/R and the activation energy can be determined. Here, a

value Ea = 246 kJ·mol^{-1} was obtained for the transformation of ettringite during the first stage. The determination of the kinetic parameters of the complete transformation would require very long experiments that are beyond the scope of the present work.

The progress of a transformation can also be described by a Time-Temperature-Transformation (TTT) diagram[49] , which indicates the time at which the transformation occurs when a sample is kept under isothermal conditions.[32] Figure 5c displays the TTT diagram determined for the beginning of the ettringite transformation (Y=10). The critical temperature ($T_c \approx 30$ºC) was estimated by running a heating and cooling cycle over a short period of time, in which no phase transformation was observed below Tc. The curve connecting the experimental data exhibit the typical shape of the TTT diagrams for transformations with increasing temperature. At low temperatures above T_c, the transformation begins after long periods of time. A further increase of temperature dramatically reduces the time over which the transformation begins.

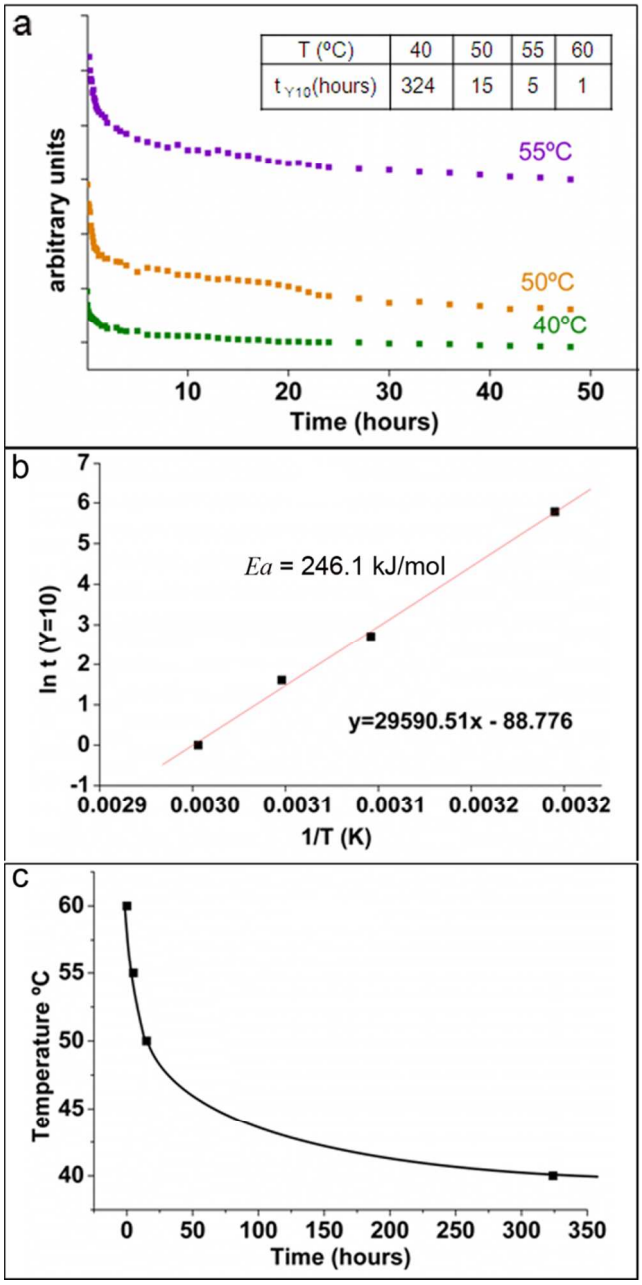

441

442 **Figure 5**. a)Variation of the peak area of the 100 reflection as a function of time during
443 three series of isothermal experiments. b) Experimental data of the time ($\ln t_{0.1}$) for a 10%
444 fraction of transformed ettringite versus $1/T$. The slope of the fitting straight line
445 corresponds to E_a/R. Time (hours) to transform a fraction (Y = 10) of ettringite. c)TTT
446 diagram corresponding to a fraction Y = 0.1 of the transformed ettringite.

Environmental implications

The capacity of the ettringite to immobilize contaminants is mostly related with its crystal structure, which allow the substitution of sulfate by oxyanions (chromate, arsenate, or selenate) and calcium by cations (lead, cadmium, cobalt). Such availability for ionic substitution suggests that ettringite-based solid-solution formation can be one of the most effective mechanisms for immobilization of pollutant ions in cements. Among the elements immobilized by ettringite, selenium is considered to have a high priority in the field of nuclear wastes due to the high toxicity of the radioisotope ^{79}Se with a half-life of $3.27\ 10^5$ years[50]. In fact, ^{79}Se is a critical radionuclide that might diffuse through the engineering and geological barriers of repositories and hence, release from waste disposals to the environment causing an increase of radiotoxicity[27] In that context, the study of the thermal stability of ettringite is crucial to understand the evolution of the crystal structure containing harmful ions and how it affects the storage environment. In the present work, the results obtained by calorimetric and thermo-XRD indicate that the dehydration/decomposition of ettringite occurs in two stages via the formation of poorly crystalline phases identified as calcium sulfates with different degrees of hydration and an amorphous phase containing aluminum. The kinetic study performed in this work is focused on the first stage and, for the first time, reveals that the initial transformation stage of ettringite occurs at relatively low temperature (40ºC). These results indicate that ettringite cannot be considered an optimum host phase for the immobilization of radionuclides and other harmful elements as frequently proposed in the literature. As long

as decomposition of ettringite exposed to atmospheric conditions is to be expected, the risk of dehydration in different long-term evolutionary scenarios deserves careful assessment.

ACKNOWLEDGMENT

This research was supported by the German Federal Ministry for Education and Research (grant 02NUK019A -IMMORAD) and the Spanish Ministry of Competitiveness and Economy (grant CGL2013- 47988-C2-2-P). Authors also thank the Amphos 21 Group for introducing us to the cement research studies.

478 REFERENCES

479 1. Hurlbut, C.; Baum, J., ETTRINGITE FROM FRANKLIN, NEW-JERSEY. *American Mineralogist*
480 **1960,** *45* (11-2), 1137-1143.
481 2. Gross, S., *The Mineralogy of the the Hatrurim Formation, Israel*. Geological Survey of
482 Israel: 1977.
483 3. Moore, A.; Taylor, H., Crystal structure of ettringite. *Acta Crystallographica Section B:*
484 *Structural Crystallography and Crystal Chemistry* **1970,** *26* (4), 386-393.
485 4. Glasser, F. In *Characterisation of the barrier performance of cements*, MRS Proceedings,
486 Cambridge Univ Press: 2002; p JJ9. 1.
487 5. Aimoz, L.; Kulik, D. A.; Wieland, E.; Curti, E.; Lothenbach, B.; Mäder, U., Thermodynamics
488 of AFm-(I_2,SO_4) solid solution and of its end-members in aqueous media. *Applied Geochemistry*
489 **2012,** *27* (10), 2117-2129.
490 6. Calvo, J. G.; Hidalgo, A.; Alonso, C.; Luco, L. F., Development of low-pH cementitious
491 materials for HLRW repositories: Resistance against ground waters aggression. *Cement and*
492 *Concrete Research* **2010,** *40* (8), 1290-1297.
493 7. Bannister, F.; Hey, M.; Bernal, J., Ettringite from Scawt Hill, Co. Antrim. *Mineralogical*
494 *Magazine* **1936,** *24* (153), 324-329.
495 8. Hartman, M.; Berliner, R., Investigation of the structure of ettringite by time-of-flight
496 neutron powder diffraction techniques. *Cement and concrete research* **2006,** *36* (2), 364-370.
497 9. Goetz-Neunhoeffer, F.; Neubauer, J., Refined ettringite (Ca6Al2 (SO4) 3 (OH) 12· 26H2O)
498 structure for quantitative X-ray diffraction analysis. *Powder diffraction* **2006,** *21* (01), 4-11.
499 10. Renaudin, G.; Segni, R.; Mentel, D.; Nedelec, J.-M.; Leroux, F.; Taviot-Gueho, C., A Raman
500 study of the sulfated cement hydrates: ettringite and monosulfoaluminate. **2007**.
501 11. Renaudin, G.; Filinchuk, Y.; Neubauer, J.; Goetz-Neunhoeffer, F., A comparative structural
502 study of wet and dried ettringite. *Cement and Concrete Research* **2010,** *40* (3), 370-375.
503 12. Evans, N., Binding mechanisms of radionuclides to cement. *Cement and concrete research*
504 **2008,** *38* (4), 543-553.
505 13. Kumarathasan, P.; McCarthy, G. J.; Hassett, D. J.; Pflughoeft-Hassett, D. F. In *Oxyanion*
506 *substituted ettringites: synthesis and characterization; and their potential role in immobilization of*
507 *As, B, Cr, Se and V*, MRS Proceedings, Cambridge Univ Press: 1989; p 83.

14. Myneni, S. C.; Traina, S. J.; Logan, T. J., Ettringite solubility and geochemistry of the $Ca(OH)_2$–$Al_2(SO_4)_3$–H_2O system at 1 atm pressure and 298 K. *Chemical Geology* **1998,** *148* (1), 1-19.

15. Baur, I.; Johnson, C. A., Sorption of selenite and selenate to cement minerals. *Environmental science & technology* **2003,** *37* (15), 3442-3447.

16. Zhang, M.; Reardon, E. J., Removal of B, Cr, Mo, and Se from wastewater by incorporation into hydrocalumite and ettringite. *Environmental science & technology* **2003,** *37* (13), 2947-2952.

17. Cornelis, G.; Johnson, C. A.; Gerven, T. V.; Vandecasteele, C., Leaching mechanisms of oxyanionic metalloid and metal species in alkaline solid wastes: a review. *Applied Geochemistry* **2008,** *23* (5), 955-976.

18. Bonhoure, I.; Wieland, E.; Scheidegger, A. M.; Ochs, M.; Kunz, D., EXAFS study of Sn (IV) immobilization by hardened cement paste and calcium silicate hydrates. *Environmental science & technology* **2003,** *37* (10), 2184-2191.

19. Bonen, D.; Sarkar, S. L. In *The present state-of-the-art of immobilization of hazardous heavy metals in cement-based materials*, Advances in cement and concrete, ASCE: 1994; pp 481-498.

20. Pinto, A. J.; Jimenez, A.; Prieto, M., Interaction of phosphate-bearing solutions with gypsum: Epitaxy and induced twinning of brushite ($CaHPO_4 \cdot 2H_2O$) on the gypsum cleavage surface. *American Mineralogist* **2009,** *94* (2-3), 313-322.

21. Prieto, M.; Astilleros, J. M.; Fernández-Díaz, L., Environmental remediation by crystallization of solid solutions. *Elements* **2013,** *9* (3), 195-201.

22. Zhou, Q.; Lachowski, E.; Glasser, F., Metaettringite, a decomposition product of ettringite. *Cement and Concrete Research* **2004,** *34* (4), 703-710.

23. Zhou, Q.; Glasser, F., Thermal stability and decomposition mechanisms of ettringite at 120 C. *Cement and concrete research* **2001,** *31* (9), 1333-1339.

24. Pourchez, J.; Valdivieso, F.; Grosseau, P.; Guyonnet, R.; Guilhot, B., Kinetic modelling of the thermal decomposition of ettringite into metaettringite. *Cement and concrete research* **2006,** *36* (11), 2054-2060.

25. Skoblinskaya, N.; Krasilnikov, K., Changes in crystal structure of ettringite on dehydration. 1. *Cement and Concrete Research* **1975,** *5* (4), 381-393.

26. Hartman, M. R.; Brady, S. K.; Berliner, R.; Conradi, M. S., The evolution of structural changes in ettringite during thermal decomposition. *Journal of Solid State Chemistry* **2006,** *179* (4), 1259-1272.

27. Wickham, S., Evolution of the near-field of the Ondraf/Niras repository concept for category C wastes. *1st full draft report, Report no. NIROND-TR* **2007**.

28. Bennett D.G., G. R., Overview of European concepts for high-level waste and spent fuel disposal with special reference waste container corrosion. *Journal of Nuclear Materials* **2008,** *379* (Issues 1–3), 1–8.

29. Ewing, R. C., Long-term storage of spent nuclear fuel. *Nature materials* **2015,** *14* (3), 252-257.

30. Verma, A. K.; Gautam, P.; Singh, T.; Bajpai, R., Numerical Simulation of High Level Radioactive Waste for Disposal in Deep Underground Tunnel. In *Engineering Geology for Society and Territory-Volume 1*, Springer: 2015; pp 499-504.

31. Blanco Martin L, R. J. B. J. T., Long-term modeling of the thermal–hydraulic–mechanical response of a generic salt repository for heat-generating nuclear waste. *Engineering Geology* **2015,** *193*, 198–211.

32. Putnis, A., *An introduction to mineral sciences*. Cambridge University Press: 1992.

33. Perkins, R. B.; Palmer, C. D., Solubility of ettringite ($Ca_6[Al(OH)_6]_2(SO_4)_3{\cdot}26H_2O$) at 5–75° C. *Geochimica et Cosmochimica Acta* **1999,** *63* (13), 1969-1980.

34. Langford, J. t.; Wilson, A., Scherrer after sixty years: a survey and some new results in the determination of crystallite size. *Journal of Applied Crystallography* **1978,** *11* (2), 102-113.

35. Atkins, M.; Macphee, D.; Kindness, A.; Glasser, F., Solubility properties of ternary and quaternary compounds in the $CaO\text{-}Al_2O_3\text{-}SO_3\text{-}H_2O$ system. *Cement and concrete research* **1991,** *21* (6), 991-998.

36. Appelo, C. A. J.; Postma, D., *Geochemistry, groundwater and pollution*. CRC Press: 2005.

37. Kulik, D. A.; Wagner, T.; Dmytrieva, S. V.; Kosakowski, G.; Hingerl, F. F.; Chudnenko, K. V.; Berner, U. R., GEM-Selektor geochemical modeling package: revised algorithm and GEMS3K numerical kernel for coupled simulation codes. *Computational Geosciences* **2013,** *17* (1), 1-24.

38. Langford, J. I.; Louer, D., Powder diffraction. *Reports on Progress in Physics* **1996,** *59* (2), 131.

39. Mittemeijer, E. J.; Scardi, P., *Diffraction analysis of the microstructure of materials*. Springer: 2004; Vol. 68.

40. Andara, A. J.; Heasman, D. M.; Fernandez-Gonzalez, A.; Prieto, M., Characterization and crystallization of Ba(SO4,SeO4) solid solution. *Crystal Growth & Design* **2005,** *5* (4), 1371-1378.

41. Delhez, R.; de Keijser, T. H.; Langford, J.; Louër, D.; Mittemeijer, E.; Sonneveld, E., Crystal imperfection broadening and peak shape in the Rietveld method. *The Rietveld method. Oxford University Press, New York* **1993**, 132-166.

42. Mittemeijer, E. J.; Welzel, U., The "state of the art" of the diffraction analysis of crystallite size and lattice strain. *Zeitschrift für Kristallographie International journal for structural, physical, and chemical aspects of crystalline materials* **2008,** *223* (9), 552-560.

43. Antao, S. M.; Duane, M. J.; Hassan, I., DTA, TG, and XRD studies of sturmanite and ettringite. *The Canadian Mineralogist* **2002,** *40* (5), 1403-1409.

44. Putnis, A.; Winkler, B.; Fernandez-Diaz, L., In situ IR spectroscopic and thermogravimetric study of the dehydration of gypsum. *Mineralogical Magazine* **1990,** *54* (374), 123-128.

45. Shimada, Y.; Young, J., Structural changes during thermal dehydration of ettringite. *Advances in cement research* **2001,** *13* (2), 77-81.

46. Skoblinskaya, N.; Krasilnikov, K.; Nikitina, L.; Varlamov, V., Changes in crystal structure of ettringite on dehydration. 2. *Cement and concrete research* **1975,** *5* (5), 419-431.

47. Lager, G.; Armbruster, T.; Rotella, F.; Jorgensen, J.; Hinks, D., A crystallographic study of the low-temperature dehydration products of gypsum, $CaSO_4 \cdot H_2O$; hemihydrate, $CaSO_4 \cdot 0.5H_2O$, and gamma-$CaSO_4$. *American Mineralogist* **1984,** *69* (9-10), 910-919.

48. Hall, C.; Barnes, P.; Billimore, A. D.; Jupe, A. C.; Turrillas, X., Thermal decomposition of ettringite $Ca_6[Al(OH)_6]_2(SO_4)_3 \cdot 26H_2O$. *Journal of the Chemical Society, Faraday Transactions* **1996,** *92* (12), 2125-2129.

49. Putnis, A.; McConnell, J., Principles Of Mineral Behaviour. **1980**.

50. Jörg, G.; Bühnemann, R.; Hollas, S.; Kivel, N.; Kossert, K.; Van Winckel, S.; Gostomski, C. L. v., Preparation of radiochemically pure 79Se and highly precise determination of its half-life. *Applied Radiation and Isotopes* **2010,** *68* (12), 2339-2351.